VIRGINIA POLYTECHNIC INSTITUTE
AND STATE UNIVERSITY

The Charles E. Via, Jr. Department
of Civil and Environmental Engineering
Blacksburg, VA 24061

Structural Engineering and Materials

STIFFNESS AND STRENGTH OF SINGLE SHEAR COLD-FORMED STEEL SCREW-FASTENED CONNECTIONS

by

Hong S. Pham, Graduate Research Assistant

Cristopher D. Moen, Ph.D., P.E.

Report No. CE/VPI-ST-15-07

June 2015

TABLE OF CONTENTS

TABLE OF TABLES

TABLE OF FIGURES

Abstract

Results are presented from an experimental program on single shear cold-formed steel-to-steel through-fastened screw connections, including documentation of the complete load-deformation response and stiffness degradation. Ply thicknesses from 0.88mm to 2.58mm and screw diameters of 4.17mm to 5.49mm were tested to cover the practical range of applications common to cold-formed steel framing. A custom non-contact optical technique measured steel ply relative displacements and screw tilting angles. Fastener load-deformation response is presented in a format that can be incorporated into codes and standards for system level design calculations that require connection stiffness to quantify load sharing. The simplified multi-linear curves characterized from monotonic responses can also serve as nonlinear springs in cold-formed steel subsystem computational models (e.g., shear wall, floor diaphragm, roof truss) and 3D whole building cold-formed steel structural simulations.

1. Introduction

Steel-to-steel screw through-fastened connections are a staple of light steel framed construction. There are thousands of fasteners in a light steel-framed building connecting studs to tracks, forming strap braced and sheathed shear walls, and attaching gypsum to interior partitions as illustrated in **Fig. 1**. Considered together, these components and their connections define building system behavior - especially lateral drift and seismic performance as demonstrated by recent full scale building tests [1].

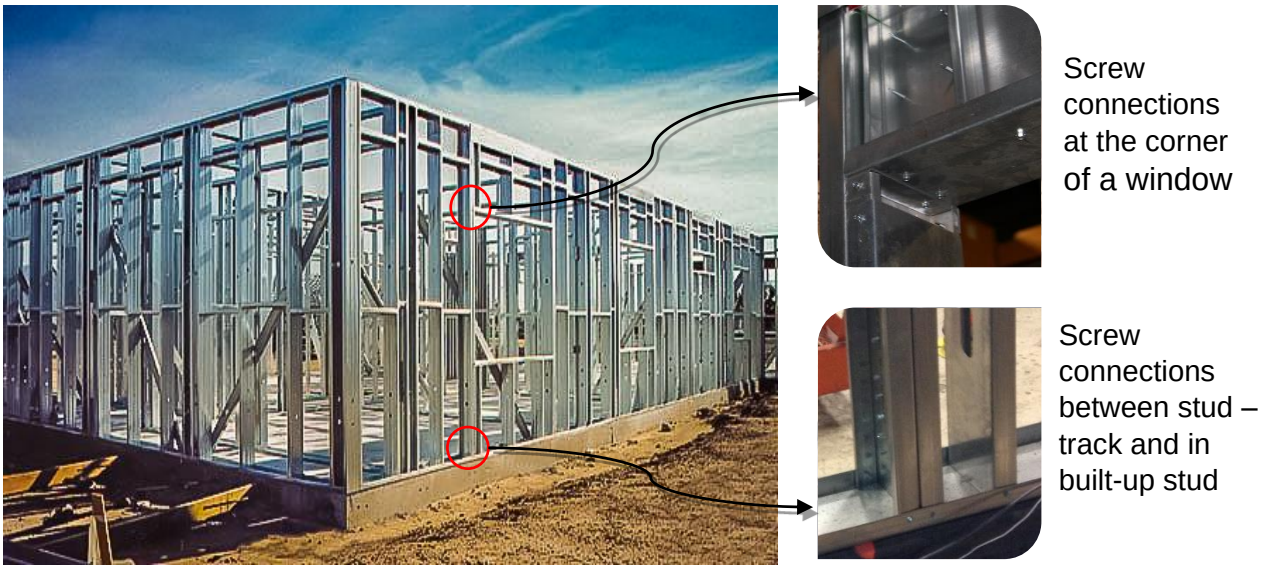

Fig. 1. Cold-formed steel building [2] and typical screw connections

Connection capacity is the focus of most cold-formed steel connection experimental programs in the literature, which is reasonable for the component level load and resistance factor approaches currently employed in design. A shift to system design is occurring however, that requires not only capacity but also stiffness and stiffness degradation with varying load. The focus of the work presented herein is to study individual steel-to-steel fastener connections and their full load-deformation response, including stiffness degradation as the connection progresses through tilting, bearing, and tearing.

2. Cold-formed steel connections: background and behavior

The current American Iron and Steel Institute (AISI) North American Specification provides steel-to-steel screw fastened capacity prediction equations ([3], Section E4.3) for tilting, bearing, and screw shear limit states that were developed by modifying existing equations in British Standards [4] and European design recommendations [5], most notably a change from ply yield strength to ultimate tensile strength that resulted in better predictions confirmed with a compilation study of over 3,500 tests [6,7]. Screw tilting and bearing strength limit states are defined in the AISI specification based on the plate thickness ratio t_2/t_1, where t_1 is the base metal thickness for the sheet ply in contact with the fastener head (referred to as ply 1) and t_2 is the base metal thickness of the connected ply typically embedded with at least one fastener thread (ply 2).

The tilting limit state is assumed to occur in the AISI capacity equations when $t_2/t_1 \leq 1.0$. Tilting is caused by the moment generated by a force couple generated in the single shear connection, and the connection failure initiates when the inclined screw tears or pulls through ply 2. A bearing failure occurs when the concentrated pressure from the fastener on ply 1 or 2 exceeds the steel yield stress causing hole elongation at a constant bearing stress, which causes the connection shear stiffness to decrease to zero. The bearing stress magnitude that causes the stiffness loss varies with fastener distance to an edge. More plate material behind the fastener increases the bearing failure pressure, a phenomenon first documented in bolted cold-formed steel connections by Winter [8]. In the study summarized herein, edge distance on the order of 10 times the fastener diameter is provided and therefore not a variable. For thicker plies (upwards of 2.58mm), local buckling deformation is minimal in front of the hole and the fastener force can spread and redistribute in the plies. However, for thinner plies (e.g., 0.88mm), local buckling decreases the ply resistance to bearing.

If both plies are sufficiently thick, the connection can carry the fastener's shear capacity that is typically documented by screw manufacturer. Tests on cold-formed steel through-fastened connections with the same ply thicknesses showed that the measured shear strength can be lower because of local ply deformation and separation that causes screw bending combined with shear [8]. When one ply is sheared and pulled relative to another, multiple strength limit states can occur at once [9], for example tilting and net section failure, tilting, bearing, and pull-out.

Recent experiments on cold-formed steel-to-steel plate screw connections by Corner [10] pointed out a key kinematics in the limit state prediction is fastener tilting. Further, it was suggested that the fastener pitch, the distance between the centerlines of two consecutive threads plays an important role in connection failure mechanism, thus should be taken into account. Haus [11] studied experimentally the monotonic and cyclic responses of steel-to-steel single screw fastened connections where two connected channel members were in either web-to-web or web-to-flange arrangements.

Simulation of cold-formed steel sub-systems such as shear walls, floor diaphragms have been ongoing actively. The numerical modelling allows investigating global behavior of systems, all limit states of individual components and the interaction among them. The simulation requires nonlinear models of framing members, screw-fastened connections and other structural components. Vieira and Schafer [12], Peterman et al [13] successfully characterized monotonic and hysteretic behavior of cold-formed steel stud-fastener-sheathing connections, providing inputs for numerical models of assemblages. Padilla [14] employed nonlinear zero length springs with parameters derived from experiments, i.e. the full load-deformation curves to model single screw-fastened connections in cold-formed sheathed shear walls.

3. Experimental program

The experimental program focuses on load-deformation response of single screw fastened cold-formed steel-to-steel connections. The plate thicknesses were selected to address all common cold-formed steel-to-steel connection limit states including tilting, bearing, combined tilting and bearing, and screw shear. The test employed hex-washer head fasteners and shank sizes of #8, #10, and #12.

3.1 Test setup

The test setup as illustrated in **Fig. 2** employed two cold-form steel sheets, 152mm wide x 203mm high each, overlapped with the lap splice length of 102mm. The two plies were fastened at the center of the overlapping area by a single screw. Ply 1 is always the ply in contact with the screw head. Each ply was bolted at its end to a 38mm thick aluminum block, which has a 102mm x 102mm opening. The test setup provided lateral restraints at the vertical plate edges consistent with a web stiffened by flanges in a cold-formed steel. A screw driven MTS Insight 150 testing machine with loading capacity of 150kN and loading rate of 0.025 mm/sec was used to perform the monotonic tests. This loading rate is consistent with that specified by the connection test standard AISI S905 [15]. Crosshead displacement was recorded by an internal LVDT with the accuracy of ±0.01 mm and applied shear force was measured with an MTS load cell with accuracy of ±1% of applied load.

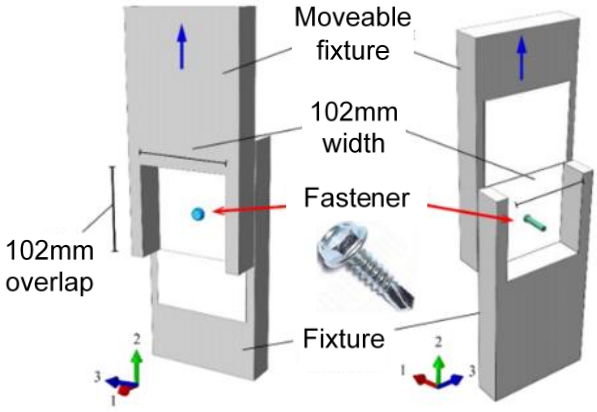

a. Front view **b**. Back view

Fig. 2. Experiment set-up

3.2 Test matrix

The experimental program test matrix is provided in **Table 1**. The test combinations were selected to cover the practical range of applications common to cold-formed steel framing, and each combination has three nominally identical tests. The specimen-naming notation defines ply 1 and 2 thicknesses in mils (33 or 0.88mm, 43 or 1.15mm, 54 or 1.44mm, 68 or 1.81mm, and 97 or 2.58 mm), screw sizes #8, #10 and #12 corresponding to the diameters of 4.17mm, 4.83mm and 5.49mm respectively, and ending with test number. For example, '9733Hex10M1' represents: w44 - internal code for the plate- plate tests, 9733 - Thicknesses (mils) of the two connected plies, ply 1 and ply 2 respectively, Hex10 - #10 hex-washer head screw type, M1 - Test #1 in the group of three 9733Hex10 Monotonic tests. For #08 and #12 screw sizes, only three test groups for each have been conducted due to time constraint.

Table 1. Test matrix

	Hex08	Hex10	Hex12
w44-3333	3	3	3
w44-3368	-	3	-
w44-4343	3	3	3
w44-4354	-	3	-
w44-4368	-	3	-
w44-4397	-	3	-
w44-5454	-	3	-
w44-6843	-	3	-
w44-9733	3	3	3
w44-9797	-	3	-

3.3 Ply material properties and base metal thickness

Web base metal thicknesses t_1 and t_2, i.e., thicknesses with zinc coating removed, yield stress F_y, and ultimate strength F_u were measured for plies 1 and 2 in each specimen. These values are reported in **Table 2** as an average of two tensile coupons per sheet measured in accordance with ASTM E8M-08 [16].

Table 2. Base metal ply thicknesses t_1 and t_2, yield stress F_y and ultimate stress F_u

Test group	t_1 (mm)	t_2 (mm)	F_{u1} (MPa)	F_{y1} (MPa)	F_{u2} (MPa)	F_{y2} (MPa)
3333	0.88	0.88	446	333	446	333
4343	1.19	1.19	456	337	456	337
9733	2.54	0.87	532	419	445	341
5454	1.41	1.41	533	453	533	453
6843	1.81	1.19	496	392	456	338
4354	1.19	1.40	456	338	531	444
3368	0.89	1.81	444	316	496	392
4368	1.19	1.83	456	338	492	376
4397	1.19	2.55	456	338	524	399
9797	2.55	2.55	523	402	523	402

3.4 Optical non-contact measurement technique

Fastener rotation and relative ply displacement were tracked using a custom optical non-contact measurement system shown in **Fig. 3**. Rods with two colored circular targets were glued at three locations on a specimen – (*i*) on the fastener head, (*ii*) at 114mm up from the Ply 1 edge, and (*iii*) 25.4mm down from the Ply 2 edge. The change in vertical displacement between (ii) and (iii) is defined as the ply relative displacement, δ. Screw rotational angle, θ, was calculated from the target coordinates on rod (i). Target motion was captured at one frame per second by two 35 mm digital SLR cameras and then post-processed using MATLAB Image Processing Toolbox [17] to track the movement of the colored targets. Optical measurement accuracy is ±0.5 mm [11].

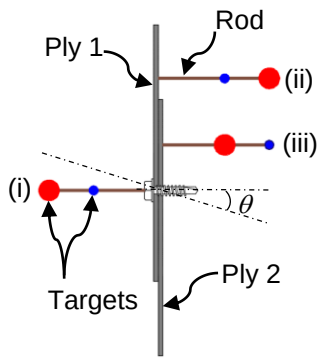

Fig. 3. Non-contact measurement set-up

4. Test results

4.1 Relative displacement

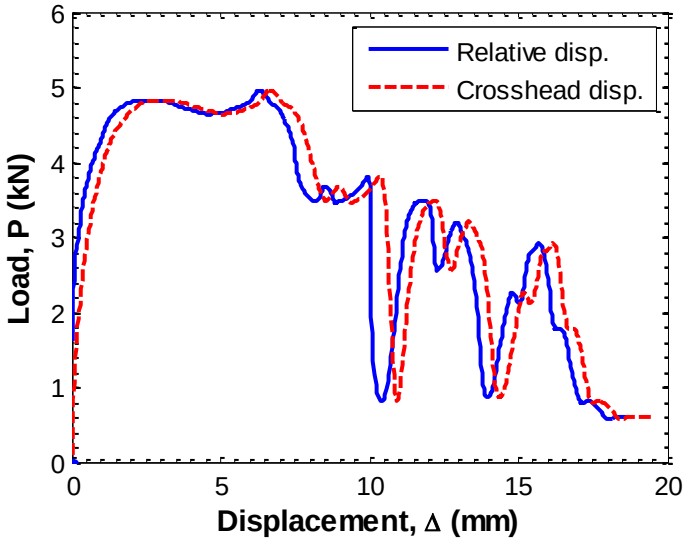

Fig. 4. Crosshead displacement vs. relative displacement for test 4343Hex10M1

Fig. 4 compares the load – displacement curves for both the crosshead and relative displacement for test 4343Hex10M1. The response associated to crosshead displacement is shown as a dashed curve, whereas the solid curve displays the relative displacement - load relationship. The ordinate represents the loads applied to the ply 1. It can be seen that, at early stages of the test where loading is small, there is essentially no difference between these displacements. However, as the load increases further, elastic deformation begins to occur and keeps developing up to a certain value. Once the load reaches the “local” yield load, based on the contact area between the screw and the corresponding ply, the curves show nonlinear behavior. This nonlinearity may also originate from the early tilting of the fastener. It is worth mentioning that the widths of plies are designed such that yielding is not able to occur across the whole ply cross- section. There is significant fluctuation after the peak for some test configurations because of following reasons. First, the fastener was pulled through the hole during those tests. However, fastener threads might grab the plies, allowing the increase of the loads before the thread was completely pulled over or deteriorated, triggering the contribution of others. Second, during the elongation of the hole, the material in front piled up, thus increased the contact area and the applied load.

4.2 Monotonic load- relative displacement curves

Representative load- ply relative displacement response is shown in **Fig. 5** for the 9733Hex10 test group. The response is linear up to 3.0kN of load and then starts softening because of the plastic deformation occurring at ply 2 where the bearing stress exceeded the value at yielding. In addition, the tilting of the fastener also contributed to the nonlinear behavior of the connection. After peak load, the response oscillates mainly due to the piling up process of the ply 2 during the elongation of the hole. The average peak load is 4.34kN, which is 28% higher than the AISI specification prediction of 3.39kN determined by Eq. E4.3.1-1 for tilting. However, the actual failure modes shown in **Fig. 6**. Failure modes for 9733 group demonstrate that the bearing capacity of ply 2 governs the overall behavior. The fastener remained mostly horizontal (θ = 2.3 degrees at the peak load) until after peak load. The fastener fractured in shear and bending at almost 15.64mm of relative ply displacement. *In this paper, the connection strength or the peak load is defined as the maximum load at the first peak in the load – deformation curve*.

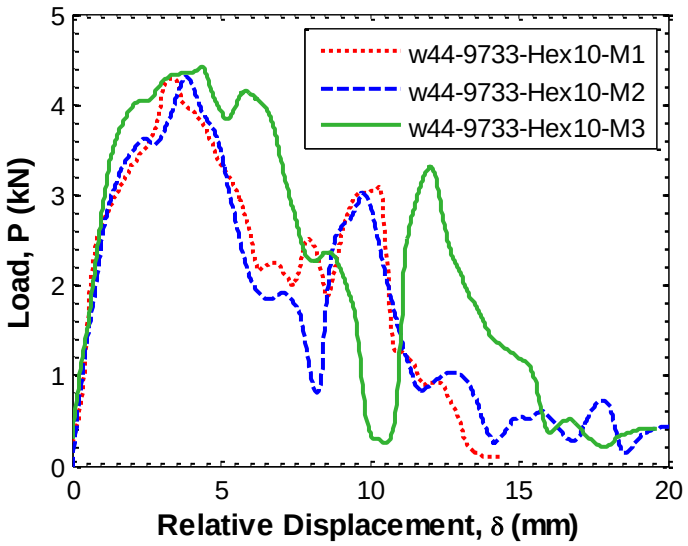

Fig. 5. Load – deformation curve for 9733 group

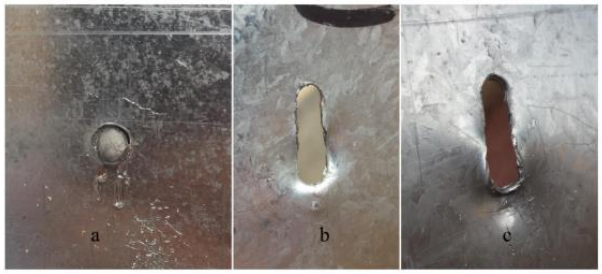

Fig. 6. Failure modes for 9733 group

a. Fastener **b.** Ply 2 – front **c.** Ply 2- back

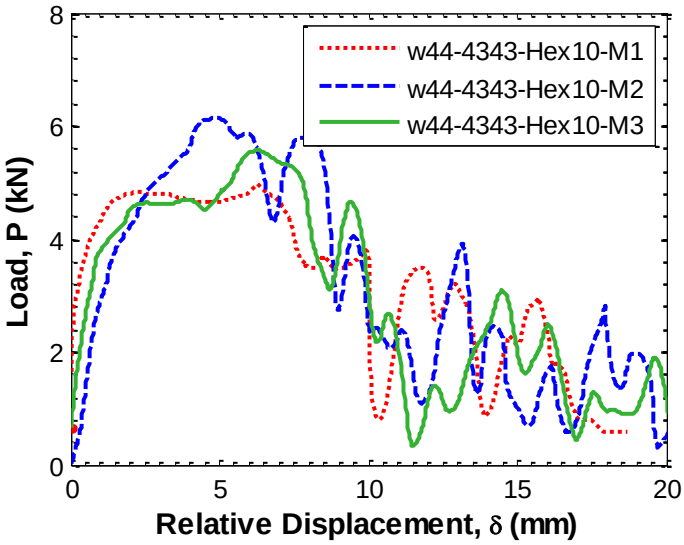

Fig. 7. Load-deformation curve for 4343 group

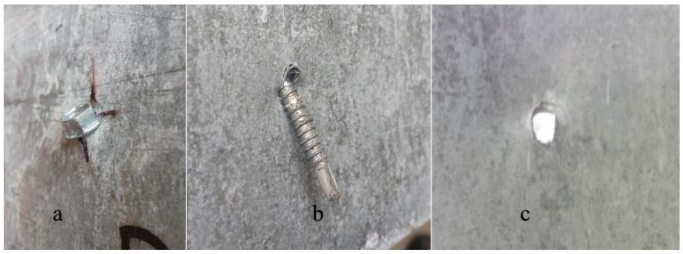

Fig. 8. Failure modes for 4343 group

a. Ply 1-front **b.** Ply 1 – back **c.** Ply 2

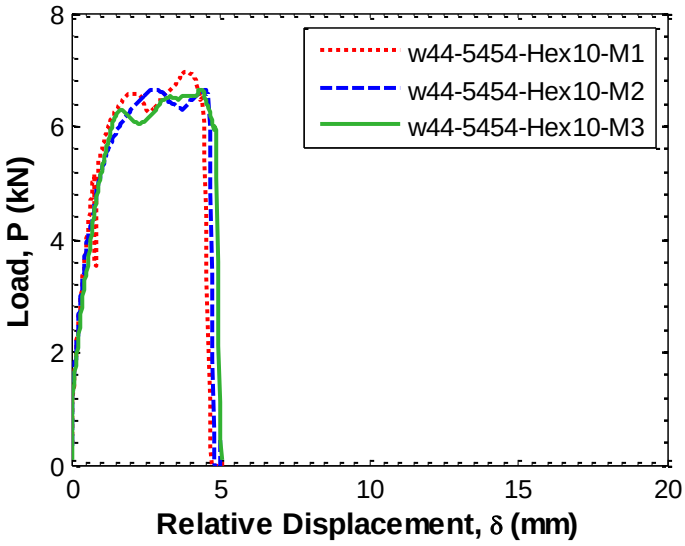

Fig. 9. Load-deformation curve for 5454 group

Fig. 10. Failure modes for 5454 group
a. Ply 1- front **b.** Ply 1 – back **c.** Ply 2- front

Load-deformation response and failure modes are compared for two similar test groups, 4343Hex10 and 5454Hex10, in **Fig. 7 - 10**. These test groups have $t_2/t_1 = 1$, however the 4343Hex10 connection accommodates 74% more relative ply displacement before failure. This is because the 4343 configuration allows more rotation and deformation at the fastener head and less bending to develop in the fastener compared to the 5454 ply (compare the average rotational angle θ = 18.8 degrees for the 4343 ply to θ = 13.0 degrees for the 5454). The 4343Hex10 average peak load is 4.87kN, which is close to the AISI predicted strength of 5.16kN using Eq. E4.3.1-1 for tilting. The average peak load for the 5454 tests is 6.75kN, higher than the 4343 since the thicker plies provide more restraint against tilting and larger contact areas with the fastener. Further, the 5454 peak load is less than the AISI prediction of 8.16kN for screw shear because of screw bending as the plies deform and separate as shown in **Fig. 10**.

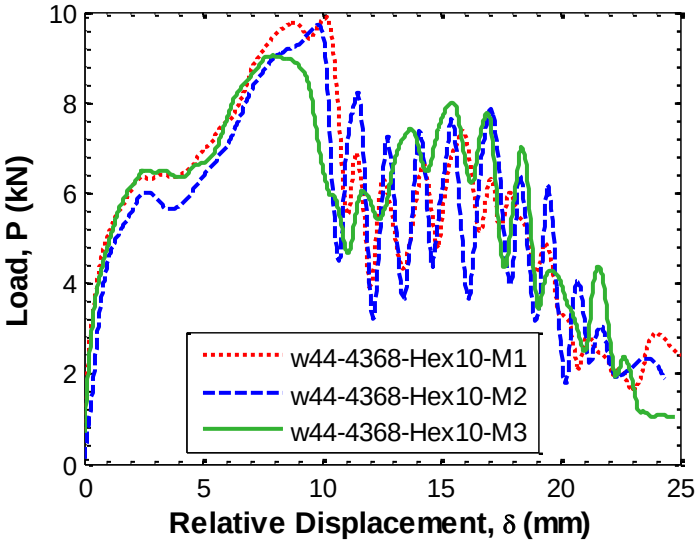

Fig. 11. Load-deformation curves for 4368 group

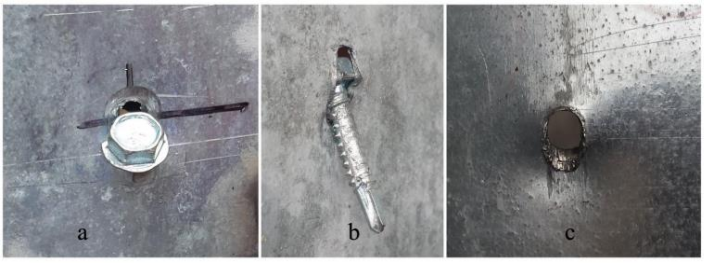

Fig. 12. Failure modes for 4368 group

a. Ply 1-front **b.** Ply 1 – back **c.** Ply 2

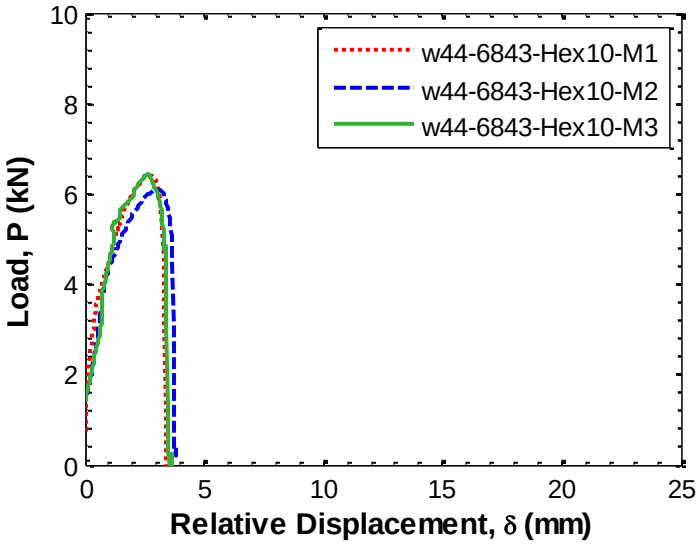

Fig. 13. Load-deformation curves for 6843 group

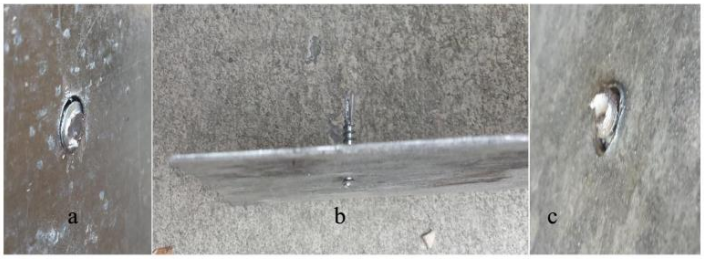

Fig. 14. Failure modes for 6843 group

a. Ply 1- back **b.** Ply 2 **c.** Ply 2- front

Fig. 11 – 14 compare the load- deformation responses and failure modes of connections with reversed ply configuration. For the 4368Hex10 group with the responses shown in **Fig. 11**, the ply 1 (43 mils) was in contact with the screw head and ply 2 (68 mils) was the connected sheet. Meanwhile, for the 6843Hex10 as displayed in **Fig. 13**, the ply 1 was the 68 mils sheet and ply 2 was the 43 mils sheet. As seen, the average peak loads and corresponding deformation capacities for the both configurations are approximately equal, but a significant post-peak response occurs in the 4368 group. The failure modes show that both tilting and

bearing followed by pullout occurs for the first group whereas primarily shear failure controls the behavior of the second group. For the 4368 group, the AISI specification predicts an ultimate strength of 6.81kN, equal to the bearing capacity of the ply 1. However, the observed average peak load was slightly smaller, equal to 6.28kN. The reduction may result from the adverse effect of fastener tilting on bearing strength. For the 6843 configuration, the AISI code assumes that tilting plays an important role in overall behavior that reduces the connection strength to 5.16kN. However, the average peak load recorded in the experiment was 25% greater (6.45kN) corresponding to a rotation angle of 9.3 degrees and the failure mode was dominated by screw shear as seen in **Fig. 14**. In this case, it is believed that tilting interacted with shearing to decrease the connection strength to the value less than the fastener shear capacity (8.16kN). Clearly, the ply configuration has a significant effect on the deformation capacities and failure modes of single fastened screw connections. The extent of its influence may vary depending on the ply thicknesses and screw sizes.

4.3 Influence of ply 1 on load-deformation response

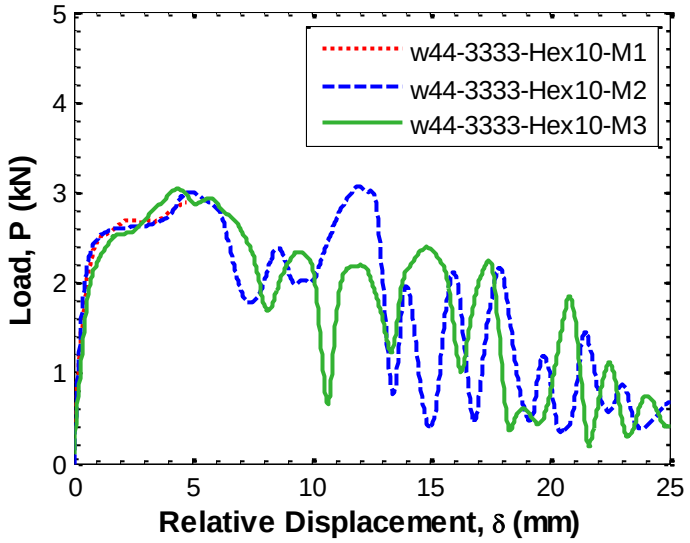

Fig. 15. Load-deformation curve for 3333Hex10 group

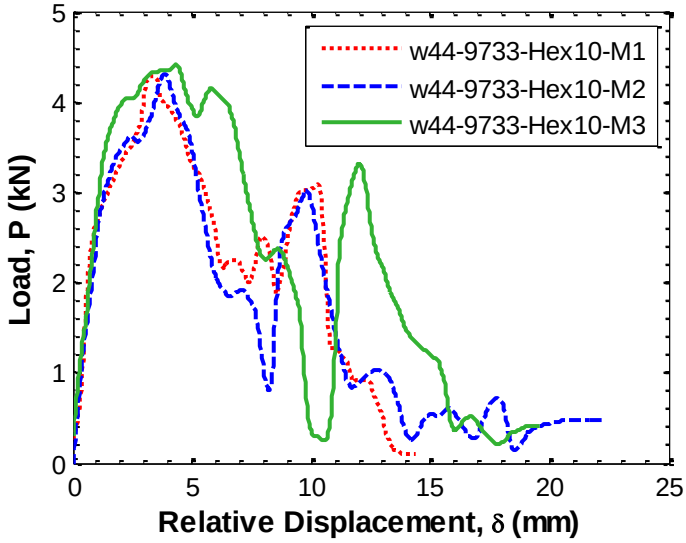

Fig. 16. Load-deformation curve for 9733Hex10 group

The load- deformation responses of two test groups with constant thickness t_2 are displayed in **Fig. 15** and **Fig. 16**. The ply 1, in contact to the screw head, provides restraints to the fastener against tilting. As tilting occurs, the upper edges of the screw head start pushing the ply 1. If the ply 1 is thin and the ratio t_2/t_1 is smaller than 2.5, the pushing force may bend the plates, allowing tilting to develop further followed by pull- out or tearing phenomena. For the 3333Hex10 group, the average rotation angle at peak load (P_{peak} = 3.07kN) was 19.5 degrees and the failure was governed by tilting. The increase of t_1 to 97mils minimized the fastener tilting (θ=2.3 degrees) and changed the failure mode to bearing of ply 2 in interaction with tilting, thus increasing the average peak load to 4.34kN. The stiffness at 40% of peak load are 4.21kN/mm and 2.81kN/m respectively for the two groups mentioned above.

4.4 Influence of ply 2 on load deformation response

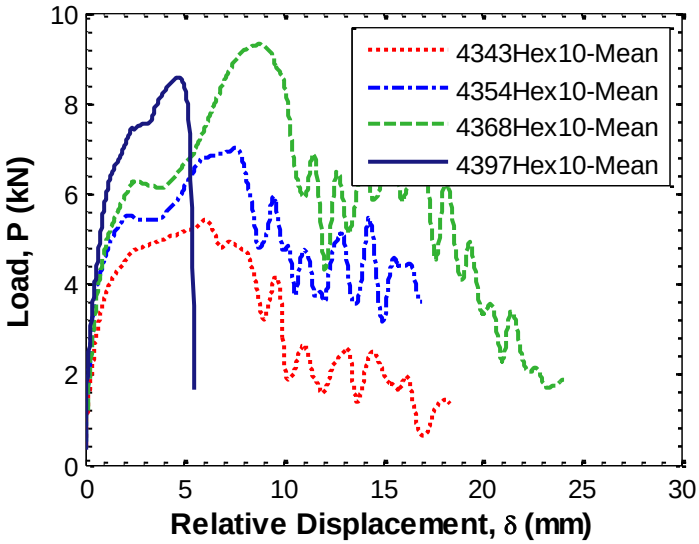

Fig. 17. 'Mean' responses of test group with constant t_1

Fig. 17 compares the "mean" responses of four test groups where the ply 1 thickness is a constant 43 mils. A mean curve of a test group is determine by averaging the three load-deformation responses of the three tests in that group. The increase of the ply 2 thickness from 43 mils to 54, 68 and 97 mils enhances the connection strength from 4.87kN to 5.54kN, 6.28kN and 8.69kN respectively. The thicker ply 2 has the similar influence on reducing the tilting of the fasteners as the thicker ply 1 does, thus gradually alters the failure modes from primarily tilting to more complex modes such as tilting and bearing or screw shear. Once the t_2 is sufficiently large (97mils), the ply 2 is able to provide restraints to keep the fastener rotated only slightly, enforces a bearing mode at the thinner sheet (43mils). If the ply 1 thickness or the contact area built-up during the test is sufficiently large as the case for 4397 group, the fastener will eventually fail in shear at a relatively small deformation as shown in **Fig. 19**. Noticeably, the stiffness at 40% of peak loads, instead of decreasing as noted in **4.3**, increases from 8.05kN/m to 8.29kN/m, 8.78kN/m and 9.28kN/m for the four groups, respectively.

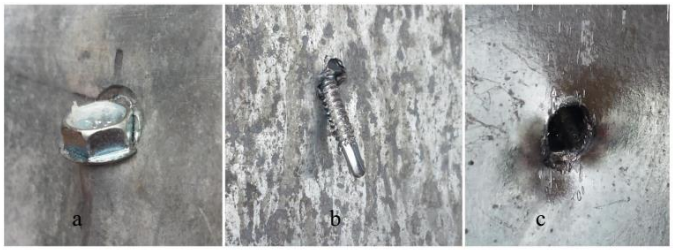

Fig. 18. Failure modes for 4354 group
a. Ply 1-front **b.** Ply 1 – back **c.** Ply 2-back

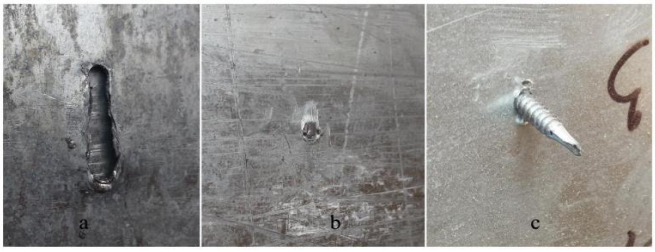

Fig. 19. Failure modes for 4397 group
a. Ply 1- front **b.** Ply 2-front **c.** Ply 2- back

4.5 Test results vs. AISI predictions

Table 4 summarizes the AISI S100-12, Section E4 connection capacity P_{AISI} for all test groups along with the corresponding average peak loads (P_{peak}) recorded from the tests. For the tests associated to #10 screw sizes which full data sets were available as shown in **Table 3**, there are two noticeable trends as follows. First, the AISI overestimates the strength of connections in which the ply ratio t_2/t_1 is in the range of 1.0 to 1.5. These tests involve those with large rotation of the fastener (3333, 4343, 4354, 4368) or primarily shear failure (9797). For the screw shear failure, as noted before, the ultimate test load did not reach the screw shear capacity provided by manufacturers (denoted as P_{ss} in AISI S100-12) since the fasteners experienced complex stress states rather than pure shear. To obtain P_{ss}, the ply thicknesses used by the manufacturer is typically 6.3 mm for plies 1 and 2, which minimize any possibility of tilting and screw bending. For those with large screw rotation, the AISI does not account for such behavior as the interaction between bearing and tilting, bending of screws, and thus over predicts the connection strength. Second, the specification underestimates the connection capacities in which the thickness ratio is either larger than 2.0 or smaller than 1.0. For relatively small t_2/t_1 ratio, the AISI predicts that either tilting or bearing governs the connection strength provided that the fastener shear failure does not occur prior to the peak load. However, the tests shown that their behavior is more complicated and affected by combined actions rather than a single mode. For instance, the 9733 has capacities associated to tilting, bearing of the two plies and screw shear are 3.39kN, 17.62kN, 5.11kN and 8.16kN respectively. Thus, according to

Table 3. Test results versus AISI predictions

t_1 (mils)	t_2 (mils)	Hex	t_2/t_1	P_{peak}/P_{AISI}
97	97	10	1.00	0.81
43	54	10	1.26	0.81
54	54	10	1.00	0.83
33	33	10	1.00	0.91
43	68	10	1.58	0.92
43	43	10	1.00	0.94
33	68	10	2.06	1.25
43	97	10	2.26	1.27
68	43	10	0.63	1.28
97	33	10	0.34	1.28

the AISI specification, its ultimate strength governed by tilting is 3.39kN. However, the average peak load observed in the test was 4.34kN. In addition, the failure mode as shown in **Fig. 6** indicated significant bearing followed by screw shear failure occurred whereas the tilting was restrained at a relative small angle of 2.3 degrees at peak load. With the thickness ratios greater than 2.0 (for 3368 and 4397 groups) but still less than 2.5, the AISI dictates an interpolation between the two cases, i.e. $t_2/t_1 \leq 1$ (tilting or bearing) and $t_2/t_1 \geq 2.5$ (bearing). The tests shown that bearing controlled the behavior along with slight tilting and even screw shear in the 4397 group. The peak loads recorded were higher than pure bearing capacity for 3368 and higher than both bearing and screw shear strength for 4397.

Table 4. Test results

Test designation	t_1		t_2		d		F_{u1}	F_{u2}	P_{peak}	P_{AISI}
	mils	mm	mils	mm	#	mm	(MPa)	(MPa)	(kN)	(kN)
w44-3333Hex08	33	0.88	33	0.88	08	4.17	446	446	3.59	3.15
w44-3333Hex10	33	0.88	33	0.88	10	4.83	446	446	3.07	3.39
w44-3333Hex12	33	0.88	33	0.88	12	5.49	446	446	3.28	3.62
w44-3368Hex10	33	0.88	68	1.81	10	4.83	446	496	6.51	5.11
w44-4343Hex08	43	1.15	43	1.15	08	4.17	456	456	5.09	4.79
w44-4343Hex10	43	1.15	43	1.15	10	4.83	456	456	4.87	5.16
w44-4343Hex12	43	1.15	43	1.15	12	5.49	456	456	5.16	5.50
w44-4354Hex10	43	1.15	54	1.44	10	4.83	456	533	5.54	6.81
w44-4368Hex10	43	1.15	68	1.81	10	4.83	456	496	6.28	6.81
w44-4397Hex10	43	1.15	97	2.58	10	4.83	456	523	8.69	6.81
w44-5454Hex10	54	1.44	54	1.44	10	4.83	533	533	6.75	8.16
w44-6843Hex10	68	1.81	43	1.15	10	4.83	496	456	6.45	5.16
w44-9733Hex08	97	2.58	33	0.88	08	4.17	523	446	2.60	3.15
w44-9733Hex10	97	2.58	33	0.88	10	4.83	523	446	4.34	3.39
w44-9733Hex12	97	2.58	33	0.88	12	5.49	523	446	4.66	3.62
w44-9797Hex10	97	2.58	97	2.58	10	4.83	523	523	6.60	8.16

5. Connection stiffness characterization

Fastener load-deformation response is generally characterized in this section, including magnitudes for initial stiffness, peak load and relative ply displacement, and equations for interpolating between ply thicknesses and screw size. Each test response is defined by four

linear legs as shown in **Fig. 20**. The first three points were pre-defined at 40%, 80% and 100% of the peak load, denoted as P_1 (d_{40}, P_{40}), P_2 (d_{80}, P_{80}), P_3 (d_{peak}, P_{peak}). The last point, P_4 (d_{final}, P_{final}) is found by matching the energy dissipated in the monotonic tests and the energy dissipated by the multi-linear model. **Table 5** in the Appendix shows the coordinates of the four points for all available monotonic tests. Generalized multi-linear load – deformation curves up to the peak are derived based on values in **Table 5**. The relationships between the normalized loads $P_i / P_{tilting}$, normalized displacements $d_i /(d.t_2/t_1)$ and a non-dimensional value of $(t_2/t_1)(d/e)(F_{u2}/F_{u1})$ have been established as shown in **Fig. 21** and **Fig. 22**. In those ratios, $P_{tilting}$ is the connection capacity determined by the AISI S100-12, Eq. E4.3.1-1 for tilting, d is the nominal screw diameter and e is the fastener thread pitch. Power regression was conducted to derive those relationships. The resulting expression are displaced adjacent to each data set as a function of ψ. For generalized connection strength, as seen in **Fig. 21**, the regression process was only applied to data with the value $\psi \geq 1.4$. The fitted curves are limited at the load ratios of 0.5, 1.0 and 1.3 corresponding to P_{40}, P_{80} and P_{peak} respectively. The test groups with capacity ratios approaching those limits include groups with the ply 1 thickness equal to 97mils, i.e. 9733Hex08-12. This is because for those configurations, the connection strength computed by the AISI specification is governed by tilting. The 9797Hex10 test group, circled in red is well below the curves since it experienced an unique failure mode – pure screw shear. Further, the 9733Hex08, circled as green also does not follow the general trend. These two special test groups may require special treatment. They were removed from the generalized connection deformation to obtain more consistent results as shown in **Fig. 22**.

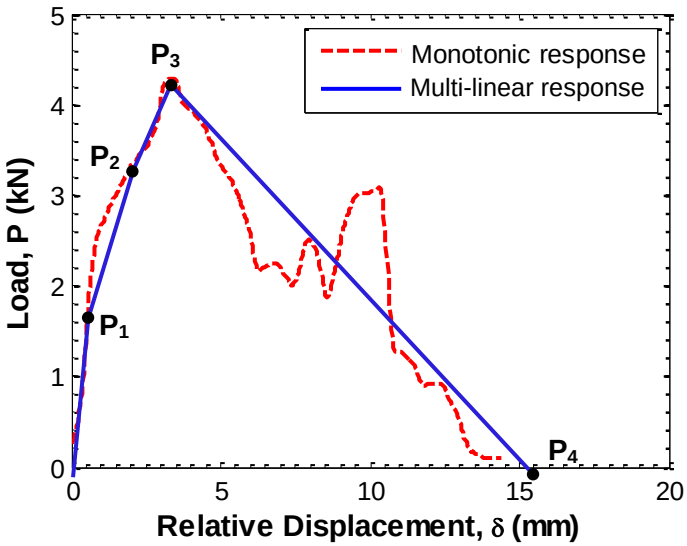

Fig. 20. Multi-linear load-deformation response

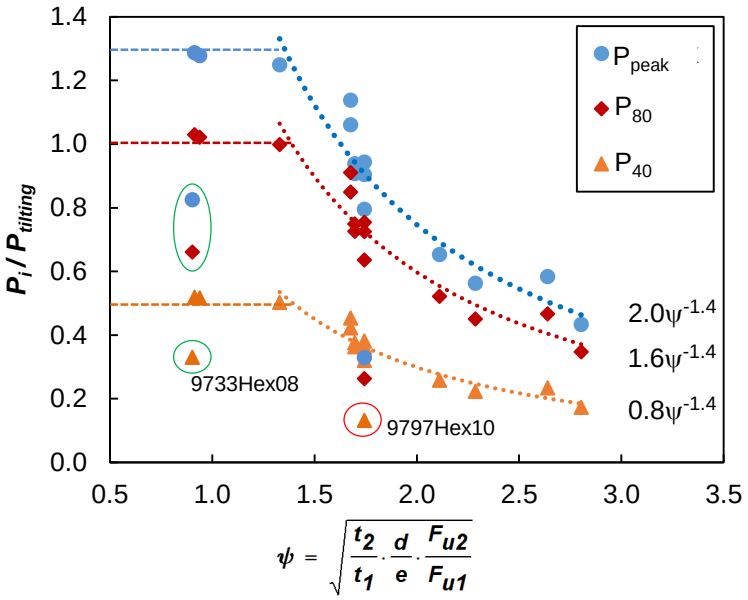

Fig. 21. Generalized connection strength

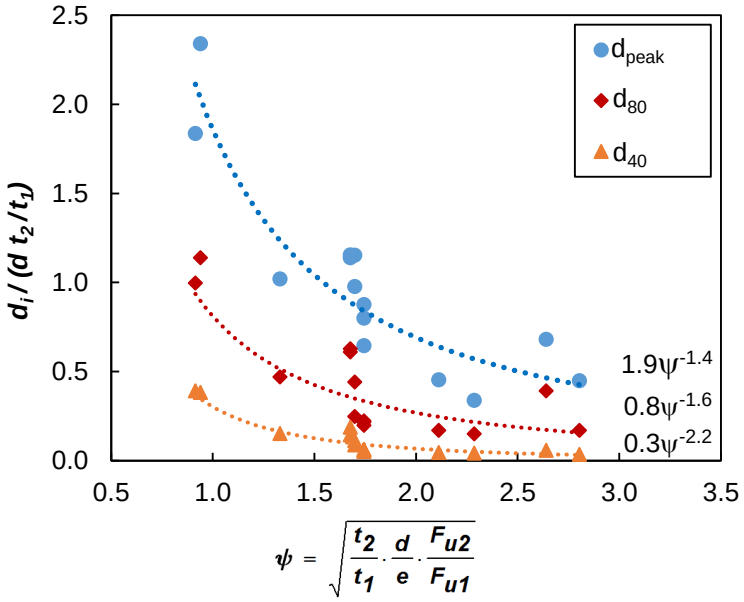

Fig. 22. Generalized connection deformation capacity

6. Conclusion

Cold-formed steel-to-steel through-fastened screw connection tests were performed to correlate existing tilting, bearing, and shear limit states to single fastener load - deformation response. Optical methods measured relative ply displacement and tracked fastener tilting angle. Experiments confirmed the essential role of the thickness ratio between the two connected plies in the connection behavior. The interaction among limit states and bending of fasteners should be accounted for in connection design. The comparison between the experimental results and coded strength proved the inconsistence of the AISI specification for certain ranges of t_2/t_1. Generalized multi-linear fastener load-deformation responses were developed for test results to serve for connection numerical modelling.

APPENDIX

Table 5. Multi-linear responses for steel-steel single screw fastened connections

Test designation	d_{40} (mm)	P_{40} (kN)	k_{40} (kN/mm)	d_{80} (mm)	P_{80} (kN)	k_{80} (kN/mm)	d_{peak} (mm)	P_{peak} (kN)	k_{peak} (kN/mm)	d_{final} (mm)	P_{final} (kN)	k_{final} (kN/mm)
w44-3333-Hex08-M1	1.37	1.48	1.08	3.45	2.97	0.72	5.26	3.72	0.42	18.79	0.00	-0.28
w44-3333-Hex08-M2	0.58	1.47	2.54	2.37	2.93	0.82	4.07	3.66	0.43	9.82	0.00	-0.64
w44-3333-Hex08-M3	0.40	1.34	3.30	2.02	2.70	0.85	5.10	3.38	0.22	17.59	0.00	-0.27
w44-3333-Hex10-M1	0.32	1.24	3.91	1.00	2.55	1.92	2.25	3.18	0.50	27.28	0.00	-0.13
w44-3333-Hex10-M2	0.24	1.24	5.22	0.81	2.40	2.03	4.92	3.00	0.15	27.08	0.00	-0.14
w44-3333-Hex10-M3	0.35	1.21	3.50	1.41	2.42	1.13	4.41	3.03	0.20	27.48	0.00	-0.13
w44-3333-Hex12-M1	0.51	1.32	2.61	4.00	2.64	0.38	5.93	3.29	0.34	24.98	0.00	-0.17
w44-3333-Hex12-M2	0.39	1.13	2.88	1.04	2.20	1.65	3.91	2.76	0.19	28.43	0.00	-0.11
w44-3333-Hex12-M3	0.98	1.49	1.53	2.22	3.04	1.25	6.26	3.80	0.19	26.41	0.00	-0.19
w44-3368-Hex10-M1	0.49	2.39	4.90	1.97	4.77	1.61	6.13	5.96	0.29	78.74	0.00	-0.08
w44-3368-Hex10-M2	0.53	2.77	5.21	2.84	5.49	1.18	5.03	6.87	0.63	55.99	0.00	-0.13
w44-3368-Hex10-M3	0.70	2.69	3.84	6.89	5.37	0.43	9.17	6.71	0.59	62.10	0.00	-0.13
w44-4343-Hex08-M1	0.88	1.76	1.99	3.68	3.55	0.64	5.06	4.44	0.64	6.90	0.00	-2.41
w44-4343-Hex08-M2	0.39	2.06	5.31	1.88	4.13	1.38	4.08	5.15	0.47	5.41	0.00	-3.89
w44-4343-Hex08-M3	0.54	2.26	4.17	2.06	4.54	1.50	5.09	5.67	0.37	10.78	0.00	-1.00
w44-4343-Hex10-M1	0.26	2.04	8.00	1.10	4.03	2.37	3.53	5.05	0.42	18.84	0.00	-0.33
w44-4343-Hex10-M2	0.27	1.89	6.92	0.91	3.70	2.85	2.58	4.64	0.56	24.73	0.00	-0.21
w44-4343-Hex10-M3	0.21	1.97	9.22	0.87	3.94	3.01	3.23	4.93	0.42	21.78	0.00	-0.27
w44-4343-Hex12-M1	0.40	1.98	4.96	0.94	3.88	3.50	6.11	4.86	0.19	19.32	0.00	-0.37
w44-4343-Hex12-M2	0.29	2.10	7.29	1.28	4.19	2.10	5.89	5.24	0.23	21.54	0.00	-0.33
w44-4343-Hex12-M3	0.78	2.14	2.74	1.87	4.31	2.00	6.99	5.38	0.21	22.67	0.00	-0.34
w44-4354-Hex10-M1	0.37	2.14	5.78	1.10	4.35	3.03	2.78	5.46	0.66	35.42	0.00	-0.17
w44-4354-Hex10-M2	0.22	2.19	9.92	1.03	4.36	2.67	3.01	5.44	0.55	32.62	0.00	-0.18
w44-4354-Hex10-M3	0.24	2.24	9.16	0.94	4.56	3.33	2.45	5.71	0.76	30.67	0.00	-0.20
w44-4368-Hex10-M1	0.21	2.49	11.85	1.02	5.08	3.20	2.47	6.34	0.87	43.97	0.00	-0.15
w44-4368-Hex10-M2	0.50	2.42	4.85	1.21	4.82	3.39	2.68	6.01	0.81	43.80	0.00	-0.15
w44-4368-Hex10-M3	0.27	2.57	9.64	1.20	5.19	2.81	2.59	6.50	0.94	42.48	0.00	-0.16
w44-4397-Hex10-M1	0.41	3.49	8.61	1.60	7.01	2.95	5.03	8.76	0.51	6.29	0.00	-6.91
w44-4397-Hex10-M2	0.31	3.31	10.71	1.11	6.79	4.33	3.92	8.47	0.60	6.47	0.00	-3.31
w44-4397-Hex10-M3	0.42	3.58	8.52	2.81	7.09	1.47	5.69	8.86	0.62	7.23	0.00	-5.75
w44-5454-Hex10-M1	0.30	2.81	9.36	1.01	5.58	3.91	3.87	6.95	0.48	5.41	0.00	-4.51
w44-5454-Hex10-M2	0.27	2.67	10.03	1.06	5.30	3.31	4.47	6.63	0.39	5.40	0.00	-7.11
w44-5454-Hex10-M3	0.33	2.66	7.95	1.07	5.31	3.63	4.35	6.65	0.41	5.78	0.00	-4.64
w44-6843-Hex10-M1	0.41	2.47	6.04	1.42	4.87	2.38	3.05	6.10	0.75	4.65	0.00	-3.81
w44-6843-Hex10-M2	0.51	2.74	5.40	1.70	5.44	2.25	3.58	6.81	0.73	5.18	0.00	-4.24
w44-6843-Hex10-M3	0.48	2.58	5.41	1.19	5.15	3.61	2.71	6.43	0.84	4.22	0.00	-4.25
w44-9733-Hex08-M1	0.07	1.11	16.97	0.34	2.15	3.83	0.96	2.69	0.87	3.32	0.00	-1.14
w44-9733-Hex08-M2	0.08	1.06	12.66	0.46	2.25	3.18	1.15	2.80	0.80	3.92	0.00	-1.01
w44-9733-Hex08-M3	0.19	0.96	5.04	0.75	1.86	1.60	1.58	2.32	0.55	4.13	0.00	-0.91
w44-9733-Hex10-M1	0.56	1.76	3.11	2.24	3.43	1.00	3.33	4.29	0.79	14.43	0.00	-0.39
w44-9733-Hex10-M2	0.70	1.75	2.51	1.97	3.45	1.33	3.84	4.31	0.46	15.02	0.00	-0.39
w44-9733-Hex10-M3	0.62	1.76	2.82	1.39	3.52	2.29	4.36	4.41	0.30	17.47	0.00	-0.34
w44-9733-Hex12-M1	0.65	1.71	2.62	1.42	3.45	2.25	3.44	4.31	0.43	40.42	0.00	-0.12
w44-9733-Hex12-M2	0.87	1.94	2.22	2.25	3.80	1.35	3.58	4.75	0.72	34.46	0.00	-0.15
w44-9733-Hex12-M3	0.66	1.98	2.97	1.91	3.92	1.56	3.27	4.90	0.72	9.77	0.00	-0.75
w44-9797-Hex10-M1	0.11	2.92	26.09	0.47	5.76	7.99	1.01	7.17	2.62	1.81	0.00	-8.85
w44-9797-Hex10-M2	0.12	2.46	20.83	0.54	4.96	5.93	0.90	6.22	3.50	1.63	0.00	-8.54
w44-9797-Hex10-M3	0.06	2.54	44.44	0.43	5.10	6.81	0.90	6.41	2.81	2.06	0.00	-5.56

REFERENCES

[1] Leng J., Schafer BW., Buonopane SG. Modeling the seismic response of cold-formed steel framed buildings: Model development for the CFS-NEES building. Struct. Stab. Res. Counc. Annu. Stab. Conf. 2013, SSRC 2013, 2013, p. 426–42.

[2] Steel IT Inc. n.d. http://steelitinc.com/ (accessed June 18, 2015).

[3] AISI. North American specification for the design of cold-formed steel structural members. 2012th ed., American Iron and Steel Institute; 2012.

[4] BSI. Structural use of steelwork in building - Part 5. Code of practice for design of cold-formed sections. 1987.

[5] ECCS. European recommendations for the design of light gage steel members. Eur. Conv. Constr. Steelwork, Brussels, Belgium: 1987.

[6] Pekoz T. Design of cold-formed steel screw connections. 10th Int. Spec. Conf. Cold-formed Steel Struct., 1990, p. 575–88.

[7] Merwe P. Development of design criteria for ferritic stainless steel cold-formed structural members and connections. Dr Diss 1987.

[8] Winter G. Tests on Bolted Connections in Light Gage Steel. J Struct Div 1956;82:1–25.

[9] Casafont M, Arnedo A, Roure F, Rodríguez-Ferran A. Experimental testing of joints for seismic design of lightweight structures. Part 1. Screwed joints in straps. Thin-Walled Struct 2006;44:197–210. doi:10.1016/j.tws.2006.01.002.

[10] Corner SMW. Screw-Fastened Cold-Formed Steel-to-Steel Shear Connection Behavior and Models. Virginia Polytechnic Institute and State University, 2014.

[11] Haus A. Energy dissipation for cold formed steel connections. Blacksburg: 2014.

[12] Vieira LCM, Schafer BW. Lateral stiffness and strength of sheathing braced cold-formed steel stud walls. Eng Struct 2012;37:205–13. doi:10.1016/j.engstruct.2011.12.029.

[13] Peterman KD, Schafer BW. Hysteretic shear response of fasteners connecting sheathing to cold - formed steel studs 2013.

[14] Padilla-llano DA. A Framework for Cyclic Simulation of Thin-Walled Cold-Formed Steel Members in Structural Systems. Virginia Tech, 2015.

[15] AISI. Test methods for mechanically fastened cold-formed steel connections. AISI S905-08 w/S1-11. 2008th ed., 2012.

[16] ASTM. Standard test methods for tension testing of metallic materials. ASTM E8/E8M-08; 2008.

[17] The MathWorks Inc. Matlab R2014a and Image Processing Toolbox n.d.